



NicE-C efficiently reveals open chromatin-associated chromosome interactions at high resolution

Zhengyu Luo, Ran Zhang, Tengfei Hu, et al.

Genome Res. published online February 1, 2022

Access the most recent version at doi:[10.1101/gr.275986.121](https://doi.org/10.1101/gr.275986.121)

P<P	Published online February 1, 2022 in advance of the print journal.
Accepted Manuscript	Peer-reviewed and accepted for publication but not copyedited or typeset; accepted manuscript is likely to differ from the final, published version.
Creative Commons License	This article is distributed exclusively by Cold Spring Harbor Laboratory Press for the first six months after the full-issue publication date (see https://genome.cshlp.org/site/misc/terms.xhtml). After six months, it is available under a Creative Commons License (Attribution-NonCommercial 4.0 International), as described at http://creativecommons.org/licenses/by-nc/4.0/ .
Email Alerting Service	Receive free email alerts when new articles cite this article - sign up in the box at the top right corner of the article or click here .



To subscribe to *Genome Research* go to:
<https://genome.cshlp.org/subscriptions>

Published by Cold Spring Harbor Laboratory Press

1 **NicE-C efficiently reveals open chromatin-associated chromosome interactions at**
2 **high resolution**

3 Zhengyu Luo^{1, 6}, Ran Zhang^{2, 6}, Tengfei Hu^{1, 6}, Yuting Zhu¹, Yueming Wu¹, Wenfei Li³, Zhi Zhang⁴, Xuebiao
4 Yao⁵, Haiyi Liang², Xiaoyuan Song¹

5
6 ¹MOE Key Laboratory for Cellular Dynamics, CAS Key Laboratory of Brain Function and Disease, School of
7 Life Sciences, Division of Life Sciences and Medicine, University of Science and Technology of China, Hefei,
8 China

9 ²CAS Key Laboratory of Mechanical Behavior and Design of Materials, Department of Modern Mechanics, Univ
10 ersity of Science and Technology of China, Hefei, China

11 ³Affiliated Psychological Hospital of Anhui Medical University, Hefei Fourth People's Hospital, Anhui Mental
12 Health Center

13 ⁴CAS Key Laboratory of Brain Function and Disease, School of Life Sciences, Division of Life Sciences and
14 Medicine, University of Science and Technology of China, Hefei, China

15 ⁵MOE Key Laboratory for Cellular Dynamics, Hefei, China, Anhui Key Laboratory for Cellular Dynamics and
16 Chemical Biology, Hefei, China 230027

17 ⁶These authors contributed equally

18 Corresponding authors: songxy5@ustc.edu.cn

19
20
21
22
23
24
25
26
27
28
29
30
31
32
33
34
35
36
37
38
39
40
41
42
43
44

45 **Abstract**

46 Enhancer-promoter communication is known to regulate spatiotemporal dynamics of gene expression.
47 Several methods are available to capture enhancer-promoter interactions, but they either require large
48 amounts of starting materials and costly, or provide a relative low-resolution in chromatin contact maps.
49 Here, we present nicking enzyme-assisted open chromatin interaction capture (NicE-C), a method that
50 leverages nicking enzyme mediated open chromatin profiling and chromosome conformation capture to
51 enable robust and cost-effective detection of open chromatin interactions at high resolution, especially
52 enhancer-promoter interactions. Using TNF stimulation and mouse kidney aging as models, we applied
53 NicE-C to reveal characteristics of dynamic enhancer-promoter interactions.

54 **Introduction**

55 Enhancers and promoters are key *cis*-regulatory elements located at open chromatin regions, which can be
56 detected by open chromatin profiling methods, such as FAIRE-seq (Giresi and Lieb 2009), DNase-seq
57 (Song and Crawford 2010), ATAC-seq (Buenrostro et al. 2013), and NicE-seq (nicking enzyme assisted
58 sequencing) (Ponnaluri et al. 2017). Long-range chromatin interactions between enhancers and promoters
59 can control cell-type- and condition-specific gene expression, which play important roles in diverse
60 biological processes, including neural development (Bonev et al. 2017), cell differentiation (Isoda et al.
61 2017), and etiopathology of diseases (Hua et al. 2018b). The development of chromosome conformation
62 capture (3C)-based methods, including Hi-C (Lieberman-Aiden et al. 2009; Rao et al. 2014) and Micro-C
63 (Hsieh et al. 2020; Krietenstein et al. 2020), has greatly promoted our understanding of high-order
64 chromatin organization and enhancer-promoter interactions. However, these genome-wide methods need
65 extremely deep sequencing to provide sufficient spatial resolution to identify enhancer-promoter
66 interactions.

67
68 To enrich *cis*-regulatory elements associated chromatin interactions, especially between enhancers
69 and promoters, methods such as Capture Hi-C (Mifsud et al. 2015), OCENA-C (Li et al. 2018), and
70 Trac-looping (Lai et al. 2018) have been developed. Although Capture Hi-C can identify genome-wide
71 chromatin interactions associated with both active and inactive promoters, it requires a costly,
72 species-specific pre-designed biotinylated RNA bait library to target known promoters. OCEAN-C and
73 Trac-looping are probe-free methods that utilize open chromatin features. OCEAN-C combines Hi-C with
74 FAIRE-seq to select open chromatin interactions, while Trac-looping uses transposase enzyme and a
75 bivalent ME linker. Although potentially very promising, Trac-looping requires about 100 million (M)
76 cells per experiment, yet identifies only a relatively low fraction of long-rang (>20 kb) *cis* chromatin
77 interactions. Limitation of OCEAN-C falls in its relative lower resolution and lower enrichment of open
78 chromatin regions. Accordingly, an improved method for capturing open chromatin interactions would be
79 highly desirable. To address these challenges, we developed a new probe-free method named NicE-C
80 (nicking enzyme assisted open chromatin interaction capture) for capturing open chromatin interactions.

81 **Results**

82 To enrich enhancer-promoter interactions in a probe-free way, we attempt to select open chromatin
83 associated chromatin interactions via combining *in situ* Hi-C (Rao et al. 2014) with open chromatin
84

85 profiling method NicE-seq (Ponnaluri et al. 2017), making full use of its limited starting materials
86 requirement and great applicability for fixed cells. In NicE-seq, a sequence-specific nicking enzyme
87 Nt.CviPII (recognizing CCD, D = A/G/T) and *E. coli* DNA polymerase I are used to label open
88 chromatin regions with biotin (Ponnaluri et al. 2017). The nicking enzyme-mediated labeling of open
89 chromatin regions also results in chromatin fragmentation at the same time, and the chromatin ends were
90 not limited to CCD (Supplemental Fig. S1A, B) (Ponnaluri et al. 2017). We found that using Nt.CviPII
91 and *E. coli* DNA polymerase I for digesting chromatin instead of using restriction enzyme in Hi-C could
92 simultaneously detect chromatin accessibility and chromatin interactions at high resolution (1-kb) (Fig.
93 1A-D). Thus, we developed NicE-C (nicking enzyme assisted open chromatin interaction capture), a
94 method that combines nicking enzyme-mediated chromatin fragmentation in NicE-seq and
95 proximity-based chromatin ends ligation in *in situ* Hi-C to specifically capture open chromatin region
96 interactions. The overall procedure of NicE-C is similar to that of *in situ* Hi-C (Fig. 1A), which begins
97 with cutting crosslinked chromatin at open regions by the nicking enzyme Nt.CviPII and *E. coli* DNA
98 polymerase I, chromatin ends are then repaired, followed by bridge linker ligation to capture open
99 chromatin interactions (Fig. 1A).

100 We first performed NicE-C with ~1 M HeLa cells. We found that both of the chromatin
101 accessibility (open chromatin) part and chromatin interaction part of NicE-C were highly reproducible
102 between biological replicates (Supplemental Fig. S1C, D). We then compared NicE-C with NicE-seq
103 data generated in-house and published ATAC-seq data (Cho et al. 2018) for HeLa cells. The results
104 showed that NicE-C efficiently captured open chromatin as evidenced by signal enrichment around both
105 promoters and enhancers, highly similar to that of NicE-seq (Fig. 1B; Supplemental Fig. S1E), and
106 about 74.2% and 82.1% of called peaks from NicE-C data overlapped with open peaks identified from
107 ATAC-seq and NicE-seq data respectively (Fig. 1C). We found that the NicE-C data showed strong
108 signal enrichment around previously reported ATAC-seq and DNase-seq peak regions, and the
109 distribution of open chromatin peaks identified by NicE-C was similar to that from the ATAC-seq and
110 DNase-seq datasets (Supplemental Fig. S1F, G). We next evaluated the capacity of NicE-C to capture
111 chromatin interactions compared to the *in situ* Hi-C data for HeLa cells and to the published Micro-C
112 data for H1-hESC cells (Krietenstein et al. 2020). NicE-C revealed chromatin organization—including
113 A/B compartments, TADs, and chromatin loops—similar to *in situ* Hi-C and Micro-C (Supplemental
114 Fig. S2A,B and S3A-C). In addition, NicE-C was able to capture fine-scale enhancer-promoter and
115 promoter-promoter interactions (E-P/P-P loops), similar to those detected with Micro-C (Hsieh et al.
116 2020; Krietenstein et al. 2020), but inefficiently with *in situ* Hi-C (Fig. 1D-F; Supplemental Fig. S2C
117 and S3D). The heatmaps indicated that NicE-C detects E-P/P-P interactions with sharp and robust signal
118 that are obviously distinct from the unclear interaction signals in the heatmaps depicting the
119 high-resolution Hi-C data (Supplemental Fig. S2C). NicE-C could detect E-P/P-P loops with much less
120 sequencing depth compared to Micro-C (Supplemental Fig. S3D), because NicE-C specifically captures
121 open chromatin interactions. We found that although NicE-C identified A/B compartments that were
122 highly similar to the Hi-C result, the E-P/P-P loops were mostly located in the A compartment; the B
123 compartment without open chromatin peaks did not have E-P/P-P loops (Supplemental Fig. S4A). Next,
124 we compared the major classes of high confidence interactions identified with NicE-C and *in situ* Hi-C

125 in HeLa cells. The majority (68.5%) of high confidence NicE-C interactions connected *cis*-regulatory
126 elements (P-P, E-P, and E-E), versus 22.1% of *in situ* Hi-C interactions (Supplemental Fig. S4B). These
127 data demonstrated NicE-C method is robust and reproducible and that NicE-C method can efficiently
128 capture open chromatin interactions at high resolution.

129 Having established that NicE-C can effectively capture open chromatin interactions, we next used
130 NicE-C to analyze human lung fibroblast cells (IMR-90) and cells from kidneys of adult female mice to
131 explore the general applicability of NicE-C. As expected, the peaks identified by NicE-C were highly
132 enriched at promoter and enhancer regions (Supplemental Fig. S5A, B). As with HeLa cells, our NicE-C
133 revealed clear enrichment of open chromatin interactions including E-P and P-P loops in IMR-90 and
134 kidney cells (Supplemental Fig. S6). We observed lines extending between E-P/P-P loops in our NicE-C
135 heatmaps and genome-wide averaged pile-up plots for all cell types (HeLa, IMR-90 and kidney cells)
136 we examined (Fig. 1D-F; Supplemental Fig. S6), which correspond to “stripes” thought to result from
137 the process of loop extrusion (Hsieh et al. 2020). Loop extrusion model explains the formation of TADs,
138 “loops” or “dots” and “stripes” or “flames” in chromatin contacts maps (Fudenberg et al. 2016; Banigan
139 et al. 2020). In loop extrusion process, once loaded onto chromatin, the *cis*-acting loop-extruding
140 factors, such as cohesin, could lead to the formation and enlargement of DNA loops that are stalled by
141 boundary elements which often bound by CTCF (Fudenberg et al. 2016). A stripe emerges when one
142 side of extruding is stalled by CTCF while the other side continues extruding (Banigan et al. 2020).

143 We further divided the enhancers and promoters of HeLa cells into four types based on whether
144 they are overlapped with CTCF or TAD boundaries. The data showed that the E-P/P-P loops or stripes
145 were stronger between enhancers and promoters overlapped with CTCF bound TAD boundaries
146 (Supplemental Fig. S7A, B), which were much weaker between enhancers and promoters overlapped
147 with neither CTCF nor TAD boundaries (Supplemental Fig. S7A, B). These results indicated that E-P
148 interactions occur in the process of loop extrusion, which can be enhanced by CTCF and/or TAD
149 boundaries. Previous studies have reported that fine-scale E-P/P-P loops and stripes are functionally
150 associated with transcription (Hsieh et al. 2020). To validate this we performed RNA-seq to correlate
151 gene expression to E-P/P-P interactions in HeLa cells. The results showed that the E-P loops and stripes
152 in our NicE-C data were highly correlated with transcription activities, where stronger interactions
153 occurred between enhancers and promoters of higher expressed genes (Supplemental Fig. S8A). This
154 was almost invisible from the Hi-C data (Supplemental Fig. S8B).

155 We next compared NicE-C with Trac-looping and OCEAN-C. We first compared random
156 convection of chromatin by identifying pairs between genomic DNA and mitochondrial DNA, which are
157 not deemed to interact with each other under normal conditions (Rao et al. 2014). The N_{nm} (reads
158 consisting of genomic DNA and mitochondrial DNA)/ N_{total} (total reads) of Trac-looping and OCEAN-C
159 were ~35 folds and ~3 folds higher than NicE-C, respectively (Supplemental Fig. S9A), indicating that
160 NicE-C minimized the artifacts from diffusion of fragmented chromatin compared with the other two
161 methods. E-P loops were reported to usually occur within the range of 1-200 kb (Hsieh et al. 2020).
162 Distribution of interaction contacts and $P(s)$ analysis showed that Trac-looping produced more
163 short-range *cis* interactions (< 20 kb), whereas OCEAN-C and Hi-C generated more long-range *cis*

164 interactions (> 20 kb), and in comparison, NicE-C generated relative even *cis* interactions in both short-
165 and long-ranges (Supplemental Fig. S9B-D).

166 Considering that the NicE-C, Trac-looping, and OCEAN-C data were generated from different
167 cells, we selected a genomic region for comparison wherein all of the cells displayed similar gene
168 expression levels based on RNA-seq. The results showed that NicE-C and Trac-looping could provide
169 informative open chromatin interactions at 1-kb resolution, while OCEAN-C provide very weak
170 interactions, if any, with the same *cis* valid pairs (Fig. 2A-D). Genome-wide analyses showed that all
171 three methods could enrich P-P loops and stripes compared to Hi-C, with NicE-C and Trac-looping
172 showing much stronger enrichment over OCEAN-C (Fig. 2E).

173 To evaluate the sensitivity of related methods, Trac-looping typically starts with 100 M cells and
174 OCEAN-C needs ~1 M cells (Lai et al. 2018; Li et al. 2018), these large amounts of starting materials
175 would limit the ability to detect the function of E-P loops in rare clinical samples. We then compared the
176 NicE-C data generated with 1 M and 0.1 M cells to check whether NicE-C could capture E-P loops with
177 reduced starting materials. Although the PCR duplication ratio was increased to ~77% for 0.1 M cells
178 compared to ~43 % for 1 M cells with a similar sequencing depth (Fig. 3A), the NicE-C data from 0.1 M
179 cells still efficiently captured similar amount of open chromatin peaks and interactions compared to
180 those from 1 M cells (Fig. 3B-E). These results suggested that NicE-C is a sensitive method to detect
181 open chromatin interactions with about 0.1 M starting cells. These results collectively support NicE-C as
182 a high-resolution, low-input and informative open chromatin interaction capture method.

183 We further explored the application of NicE-C to detect changes in E-P loops between different
184 cellular states. Specifically, we performed NicE-C and RNA-seq for HeLa S3 cells with or without TNF
185 stimulation or on young versus old mouse kidney tissues. We found that 223 genes increased expression
186 after TNF stimulation, while only 38 genes down regulated. Compared to unchanged genes, the
187 promoters of up-regulated genes showed increased enrichment of chromatin interactions with enhancers
188 or other promoters in TNF-stimulated cells (Supplemental Fig. S10A, B). As one specific example, the
189 *TNFAIP3* gene ("TNF alpha induced protein 3") displayed a ~200 folds induction upon TNF stimulation
190 according to our RNA-seq data (Fig. 4A). The NicE-C data showed that the promoter of *TNFAIP3*
191 formed multiple interactions with nearby enhancers, which were not detectable in untreated control cells
192 (Fig. 4A). Relative to young mouse kidney tissues, we identified 310 up-regulated genes and 257
193 down-regulated genes in old kidney tissues, consistent with previous findings that kidney aging
194 accompanied with increased immune infiltration, decreased mitochondrial function, and significantly
195 upregulated transporter genes on the apical side (Takemon et al. 2021). We found that the promoters of
196 up- or down-regulated genes tend to interact with enhancers or other promoters with more or less
197 frequency (Supplemental Fig. S10C-F). For examples, the promoter of down-regulated gene *AcsM3*
198 (acyl-CoA synthetase medium chain family member 3), which encoded a protein located to
199 mitochondria, showed decreased interactions with nearby enhancers in old kidney compared to those in
200 young kidney (Fig. 4B). The promoter of the up-regulated gene *Slc7a12* (solute carrier family 7,
201 member 12), belonging to transporter genes on the apical side, formed more interactions with nearby
202 enhancers in old kidney compared to those in young kidney (Supplemental Fig. S11). These results

203 demonstrated that NicE-C can detect dynamic E-P loops that are tightly linked to gene transcription
204 changes.

205

206 **Discussion**

207 Enhancer-promoter communications play critical roles in transcription regulation (Rao et al. 2014;
208 Bonev et al. 2017; Weintraub et al. 2017; Hua et al. 2018a). However, current methods for detecting E-P
209 interactions are not convenient or efficient, limiting their ability to study the function and dynamic of
210 E-P interactions during biological processes or diseases. Here, we have established a high resolution
211 NicE-C method for *cis*-regulatory elements associated chromatin interactions capture, especially the
212 interactions between enhancers and promoters, from 0.1 to 1 M cells at 1-kb resolution. We showed that
213 NicE-C can detect E-P/P-P loops and stripes, and these interactions are tightly linked to gene
214 transcription. NicE-C is an easy-to-operate method as the overall procedure of NicE-C is similar to that
215 of Hi-C, with nicking enzyme mediated open chromatin digestion replacing restriction enzyme in Hi-C.
216 In addition, NicE-C is also a time-saving method which can be finished in 2 days, compared to 3 days
217 for Ocean-C and 4 days for Trac-looping.

218 Dynamic chromatin interactions of *cis*-regulatory elements in the nucleus pose a challenge for
219 studying diseases as non-coding risk variants often locate far from their regulated genes. Previous
220 studies based on promoter capture Hi-C showed that promoter-associated chromatin interactions could
221 link non-coding GWAS (genome-wide association studies) variants with putative target genes and the
222 promoter-interacting regions enriched for eQTLs (expression quantitative trait loci) (Javierre et al. 2016),
223 revealing the unique value of *cis*-regulatory elements interaction in elucidating disease etiology. Clinical
224 samples from patients are often limited, thus the genome-wide promoter capture Hi-C (~ 20 M cells) and
225 Trac-looping (~100 M cells) are not suitable for detecting the dynamics of E-P interactions associated
226 with diseases. Ocean-C could start with ~1 M cells, but the resolution of *cis*-regulatory elements
227 associated interactions detected by Ocean-C is relatively lower compared to other methods. We have
228 showed that NicE-C can be used to informatively track dynamic changes of E-P/P-P loops across
229 different cellular conditions with limited starting materials. We thus believe that NicE-C is more
230 appropriate for studying *cis*-regulatory elements associated interactions in disease.

231 We demonstrated that NicE-C is an easy-to-implement, time-saving and efficient method for
232 profiling E-P loops at high resolution. Although NicE-C requires the least starting materials among
233 published open chromatin associated chromatin interaction capture methods, it is still not compatible
234 with single-cell profiling. Further optimization still needed to push the NicE-C method in delineating
235 open chromatin interactions and precision E-P communications to single cell levels.

236

237 **Methods**

238 **Cells and animals**

239 HeLa cells, HeLa-S3 cells and IMR-90 cells were grown in DMEM medium containing 10% fetal
240 bovine serum (FBS) at 37°C and 5% CO₂. The cells were cultured to 70%-80% confluence and then
241 used for further experiments. C57BL/6 mice were originally purchased from Vital River Laboratories in
242 Beijing, China. The mice were housed in the Animal Center of the University of Science and

243 Technology of China and were cultured under a 12-h light/dark cycle (lights off at 7 p.m.) at $23\pm 2^{\circ}\text{C}$.
244 All animal experiments were carried out in accordance with the guidelines of and approved by the
245 University of Science and Technology of China (USTC) Animal Resources Center and University
246 Animal Care and Use Committee (permit number: USTCACUC1801015).

247

248 **Cell treatment and crosslink**

249 For crosslinking, cultured cells were collected by trypsin and then fixed at room temperature for 10 min
250 with 1% formaldehyde (Sigma-Aldrich, F8775-500ML). After crosslinking, adding 2.5 M Glycine
251 (Sigma-Aldrich, G8898-1KG) to final 125 mM and incubated at room temperature for 10 min to quench
252 the reaction. Fixed cells were pelleted and washed twice with ice-cold $1\times$ PBS. After removing the
253 supernatant, the fixed cells were stored at -80°C until used. TNF (Sino biological, 10602-HNAE) was
254 dissolving in water to a final concentration of 20 ng/ μl . Cultured HeLa-S3 cells were washed once with
255 $1\times$ PBS, and fresh DMEM media supplemented with final 10 ng/ml TNF or water were added. Cells
256 were then incubated for 60 min and subjected to NicE-C or RNA-seq.

257

258 **Dissociation of cells from mouse kidneys**

259 Mouse kidneys were dissected and minced to small pieces by surgical scissors in ice-cold $1\times$ PBS and
260 were transferred to the top of a 40 μm cell strainer (Sorfa, 251100) and pelleted at 500 g for 3 min at
261 4°C . The cells were fixed at room temperature for 10 min with 1% formaldehyde. After crosslinking,
262 final 125 mM Glycine was added and incubated at room temperature for 10 min to quench the reaction.
263 Fixed cells were pelleted and washed twice with ice-cold $1\times$ PBS. After removing the supernatant, the
264 fixed cells were stored at -80°C until used.

265

266 **NicE-seq library preparation**

267 NicE-seq was performed following the published protocol with slight modifications (Ponnaluri et al.
268 2017; Chin et al. 2020). In brief, one million fixed cells were resuspended in 1 ml of cytosolic buffer (15
269 mM Tris-HCl pH 7.5, 5 mM MgCl_2 , 60 mM KCl, 0.5 mM DTT, 15 mM NaCl, 300 mM sucrose, and 1%
270 NP-40), incubated on ice for 10 min and pelleted at 800 g for 3 min at 4°C . The pellet was resuspended
271 in the following reaction: 0.5 μl of Nt.CviPII (NEB, R0626S), 2 μl of DNA Polymerase I (NEB,
272 M0209L), 3 μl of 1 mM dTTP, dGTP, biotin-14-dATP (Jena Bioscience, NU-835-BIO14-S) and 1.5 μl
273 of 1 mM biotin-14-dCTP (Jena Bioscience, NU-956-BIO14-S), 5-methyl-dCTP (NEB, N0356S), 40 μl
274 50% PEG8000 in 200 μl $1\times$ NEBuffer2. The nuclei were incubated at 37°C for 25 min for open
275 chromatin labeling with interval shaking (950 rpm, 15 s every 2 min). The nuclei were pelleted at 800 g
276 for 3 min, then resuspended in 300 μl reverse crosslinking buffer (20 mM Tris pH 8.0, 20 mM NaCl,
277 0.1% Triton X-100, 15 mM DTT, 1 mM EDTA) containing 10 μl Proteinase K (Thermo Fisher
278 Scientific, EO0492) and incubated at 65°C for overnight. DNA were purified with HiPure Gel Pure
279 DNA Mini Kit (Magen, D2111-03) and then sonicated to 200 to 400 bp fragments. The DNA fragments
280 were then mixed with 30 μl of washed Dynabeads M-280 (Thermo Fisher Scientific, 11205D) and
281 incubated at room temperature for 30 min for open chromatin selecting with slow rotation. End repair,
282 dATP tailing, adapter ligation and PCR amplification were performed with selected DNA sequentially.

283 The PCR products were size selected with VAHTS DNA Clean Beads (Vazyme, N411-01), and the
284 libraries were sequenced via Illumine NovaSeq platforms.

285

286 **Bridge linker preparation for NicE-C**

287 For NicE-C bridge linker ligation, three biotinylated bridge linkers:

288 Bridge linker B1: 5'-[5Phos]TGCGGA/iBIOdT/CCGCAT-3',

289 Bridge linker B2: 5'-[5Phos]ACCGGA/iBIOdT/CCGGTT,

290 Bridge linker H: 5'-[5Phos]TGCAAGCT/iBIOdT/GCAT,

291 with the 3' nucleotide T over-hanging on both strands after annealing were used (NicE-C libraries
292 prepared with Bridge linker B1 and B2 can be digested with BamHI to estimate the portion of
293 biotinylated junctions, NicE-C libraries prepared with Bridge linker H can be digested with HindIII to
294 estimate the proportion of biotinylated junctions). Bridge linkers were dissolved in 1× NEBuffer2 to a
295 concentration of 100 μM and annealed on the PCR machine as follows: 95°C for 2 minutes, then hold
296 for 30 seconds at each cycle with a drop of 0.5°C/cycles for 140 cycles to final 25°C. The annealed
297 Bridge linkers were stored at -20°C.

298

299 **NicE-C library preparation**

300 *Chromatin digestion*

301 One million or 0.1 million fixed cells were resuspended in 1 ml of cytosolic buffer (15 mM Tris-HCl pH
302 7.5, 5 mM MgCl₂, 60 mM KCl, 0.5 mM DTT, 15 mM NaCl, 300 mM sucrose, and 1% NP-40),
303 incubated on ice for 10 min and pelleted at 800 g for 3 min at 4°C. The pellet was resuspended in the
304 following reaction: 0.5 μl of Nt.CviPII (NEB, R0626S), 2 μl of DNA Polymerase I (NEB, M0209L), 3
305 μl of 1 mM dTTP, dGTP and dATP, 1.5 μl of 1 mM dCTP and 5-methyl-dCTP (NEB, N0356S), 40 μl
306 50% PEG8000 in 200 μl 1× NEBuffer2. The nuclei were incubated at 37°C for 25 min for chromatin
307 digestion at open region with interval shaking (950 rpm, 15 s every 2 min). 500 mM EDTA was added
308 to final 30 mM and incubated at 65°C for 20 min to stop the reaction, then the nuclei were pelleted at
309 800 g for 2 min.

310 *Troubleshooting*

311 The chromatin digestion efficiency is important for NicE-C. To determine the efficacy of chromatin
312 digestion at open chromatin regions, take 20 μl of digested cells from the previous step. Add 170 μl
313 reverse crosslinking buffer and 10 μl Proteinase K, incubate at 65°C for 30 to 60 min. Then purify DNA
314 with HiPure Gel DNA Mini Kit and check the quality of chromatin digestion by running the purified
315 DNA on a 1 % agarose gel. The sample is properly digestion if one sees a large smear of DNA
316 fragments between ~4 kb to 12 kb (see Supplemental Fig. S1A, 20 min). We recommend characterizing
317 NicE-C chromatin digestion efficiency when performing the NicE-C with a new cell type or new tissue
318 sample. In the event of over-digestion of chromatin, we recommend optimizing the amount of Nt. CviPII
319 and DNA Polymerase I used, or the digestion time.

320 *Chromatin end repair and dA-tailing*

321 After chromatin digestion and reaction stop, washing twice with NicE-C wash buffer (2 mM MgCl₂, 1×
322 BSA, 2.5% PEG8000, 0.05% SDS, 0.2% Triton X-100), the nuclei were resuspended in 400 μl 1 x T4

323 ligase buffer containing 20 μ l of 10% Triton X-100, 20 μ l of 50% PEG8000, 10 μ l of 10mM dNTPs, 10
324 μ l of T4 Polynucleotide Kinase (NEB, M0201S), 8 μ l of T4 DNA Polymerase (NEB, M0203S), 2 μ l of
325 Klenow (NEB, M0210S). Then, the nuclei were incubated at 37°C for 60 min for end repair with
326 interval shaking (950 rpm, 15 s every 2 min). 500 mM EDTA was added to final 30 mM and incubated
327 at 65°C for 20 min to stop the reaction. After washing twice with NicE-C wash buffer, the nuclei were
328 resuspended in 400 μ l 1 \times NEBuffer2 containing 20 μ l of 10% Triton X-100, 20 μ l of 50% PEG8000,
329 10 μ l of 10 mM dATP, 10 μ l of Klenow (exo-) (NEB, M0212S). Then, the nuclei were incubated at
330 37°C for 60 min for dA tailing with interval shaking (950 rpm, 15 s every 2 min). 500 mM EDTA was
331 added to final 30 mM and incubated at 65°C for 20 min to stop the reaction.

332 ***Chromatin ligation with biotin-labeled Bridge linker***

333 After dA-tailing and reaction stop, washing twice with NicE-C wash buffer, the nuclei were resuspended
334 in 600 μ l 1 \times T4 DNA ligase buffer containing 30 μ l of 10% Triton X-100, 30 μ l of 50% PEG8000, 20
335 μ l of 50 μ M Bridge linker, 4 μ l of T4 DNA ligase (NEB, M0202S). Then, the nuclei were incubated at
336 23°C for 4 hours for proximity ligation with interval shaking (1100 rpm, 15 s every 2 min).

337 ***Sequencing library generation***

338 For starting with 1 M or more cells: after ligation, reverse crosslinking, DNA purification, DNA
339 fragmentation were performed sequentially. The DNA fragments were then mixed with 30 μ l of washed
340 Dynabeads M-280 and incubated at room temperature for 30 min for biotin labeled fragments selecting
341 with slow rotation. End repair, dATP tailing, adapter ligation and PCR amplification were performed
342 with selected DNA sequentially. The PCR products were size selected with VAHTS DNA Clean Beads
343 (Vazyme, N411-01), and the libraries were sequenced via Illumine NovaSeq platforms.

344 For starting with 0.1 M cells: after ligation and reverse crosslinking, sonication was used to shear the
345 DNA without DNA purification to reduce the loss of DNA. After sonication, the DNA fragments in
346 reverse crosslinking buffer were then mixed with 10 μ l of washed Dynabeads M-280 and incubated at
347 room temperature for 30 min for biotin labeled fragments selecting with slow rotation. End repair, dATP
348 tailing, adapter ligation and PCR amplification were performed with selected DNA sequentially. The
349 PCR products were size selected with VAHTS DNA Clean Beads (Vazyme, N411-01), and the libraries
350 were sequenced via Illumine NovaSeq platforms.

351

352 ***In situ Hi-C library preparation***

353 *In situ* Hi-C was performed following the published protocol with slight modifications (Rao et al. 2014).
354 In brief, one million fixed cells were resuspended in 1 ml of ice-cold Hi-C lysis buffer (10 mM Tris, pH
355 8.0, 10 mM NaCl, 0.2% Igepal CA-630 and 1 \times complete protease inhibitors) and incubated on ice for
356 15 min. The nuclei were pelleted and resuspended in 50 μ l of 0.5% (w/v) SDS (Thermo Fisher
357 Scientific, 24730020), incubated at 62°C for 10 min. Then, 25 μ l 10% (v/v) Triton X-100
358 (Sigma-Aldrich, X100-100ML) and 145 μ l of water were added to the tube and incubated at 37°C for 10
359 min with shaking to quench SDS. The volume was brought to 400 μ l with final 1 \times NEBuffer2
360 containing 200 U of MboI (NEB, R0147M) and incubated at 37°C overnight for chromatin digestion
361 with shaking at 900 rpm. The next day, incubated at 62°C for 20 min to inactivate MboI. Then,
362 biotin-14-dATP (Jena Bioscience, NU-835-BIO14-S), dCTP, dTTP, dGTP and Klenow (NEB, M0210S)

363 were added for biotin fill in by incubating at 37°C for 90 min. Then 10× T4 DNA ligase buffer, 100×
364 BSA, 10% Triton X-100 and T4 DNA ligase (NEB, M0202S) were added for proximity ligation by
365 incubating at 25°C for 4 hours with slow rotation. After ligation, reverse crosslinking, DNA purification,
366 DNA fragmentation were performed sequentially. The DNA fragments were then mixed with 30 µl of
367 washed Dynabeads M-280 and incubated at room temperature for 30 min for biotin labeled fragments
368 selecting with slow rotation. End repair, dATP tailing, adapter ligation and PCR amplification were
369 performed with selected DNA sequentially. The PCR products were size selected with VAHTS DNA
370 Clean Beads (Vazyme, N411-01), and the libraries were sequenced via Illumine NovaSeq platforms.

371

372 **RNA-seq**

373 One million TNF treated, control HeLa-S3 cells or dissociated mouse kidney cells were collected
374 respectively and resuspended in 1 ml of TRIzol (Invitrogen, 15596018) according to the manufacturer's
375 instructions. RNA purification and sequencing library construction were performed by Berry Genomics,
376 then the libraries were sequenced via Illumine NovaSeq platforms.

377

378 **NicE-C, NicE-seq and ATAC-seq peak identification and correlation analysis**

379 We mapped NicE-C, NicE-seq reads and published ATAC-seq data (Cho et al. 2018) to hg19 or mm9
380 genome by Bowtie 2. We also mapped the reads of some samples to hg38 or mm10 and found that their
381 genome-wide profiles are highly similar to that mapped to hg19 or mm9. Thus, we believe that the use
382 of hg19 or mm9 in this study would not affect the conclusion. MACS2 (Zhang et al. 2008) was used to
383 call peaks. Overlap of Open chromatin peaks in ATAC-seq, NicE-seq and NicE-C were identified using
384 BEDTools (Quinlan and Hall 2010). Sample correlations were analyzed based on the output of
385 multiBamSummary function of deepTools (Ramírez et al. 2014) and Spearman method was used to
386 compute correlation coefficients. The intersect function of BEDTools was used to count the number of
387 reads mapped to each peak. The count matrix was normalized by Reads Per Million (RPM) mapped
388 reads. Pearson correlation coefficients between biological replicates of mouse kidneys NicE-C were
389 calculated based on the \log_{10} RPM matrix.

390

391 **ChIP-seq analysis**

392 Public H3K27ac and H3K4me3 ChIP-seq datasets of HeLa cell and IMR-90 cell (GSM1670864,
393 GSM1670868, GSM1846779, GSM1846782, GSM2774992, GSM2774993, GSM2774994,
394 GSM2774995, GSM1055816) were mapped to hg19 genome by Bowtie 2. We also mapped the reads of
395 some samples to hg38 and found that their genome-wide profiles are highly similar to that mapped to
396 hg19. Thus, we believe that the use of hg19 in this study would not affect the conclusion. Peaks were
397 called by MACS2 peak analysis function. Regions with H3K27ac enrichment but without H3K4me3
398 enrichment were identified as enhancer regions.

399

400 **RNA-seq analysis**

401 The FASTQ files of RNA-seq were mapped to the human genome (hg19) or mouse genome (mm9) with
402 HISAT2 (Pertea et al. 2016). We also mapped the reads of some samples to hg38 or mm10 and found

403 that their genome-wide profiles are highly similar to that mapped to hg19 or mm9. Thus, we believe that
404 the use of hg19 or mm9 in this study would not affect the conclusion. Counts per gene were determined
405 with HTSeq (Anders et al. 2015). Genes with significantly (Fold Change > 2, P -adj < 0.05) increased or
406 decreased expression levels after TNF treatment or during mice aging process were identified with
407 DESeq2 (Love et al. 2014).

408

409 **Mapping, pairing, and browsing of NicE-C and Hi-C data**

410 Valid NicE-C and Hi-C contact read pairs were obtained from HiC-Pro (Servant et al. 2015). Briefly,
411 paired-end reads were mapped to hg19 or mm9 reference genome separately by Bowtie 2 (Global option:
412 --very-sensitive -L 30 --score-min L,-0.6,-0.2 --end-to-end --reorder, local option: --very-sensitive -L 20
413 --score-min L,-0.6,-0.2 --end-to-end --reorder) (Langmead and Salzberg 2012). We also mapped the
414 reads of some samples to hg38 or mm10 and found that their genome-wide profiles are highly similar to
415 that mapped to hg19 or mm9. Thus, we believe that the use of hg19 or mm9 in this study would not
416 affect the conclusion. To rescue the chimeric fragments spanning the ligation junction, the ligation site
417 was detected and the 5' end fraction of the reads was aligned back to the reference genome. Pairs with
418 multiple hits, low MAPQ, singleton, dangling end, self-circle, and PCR duplicates were removed.
419 Output files containing all valid pairs were used in downstream analyses. The reproducibility of NicE-C
420 and Hi-C valid pairs were evaluated by Hi-Rep (Yang et al. 2017). For the downstream analysis, valid
421 pairs obtained from biological replicates were pooled as the biological replicates showed high
422 reproducibility. The valid pairs were then converted to HIC files using hicpro2juicebox.sh, provided by
423 HiC-Pro for visualization with Juicebox (Durand et al. 2016) or WashU Epigenome Browser (Li et al.
424 2019). We selected equal number of *cis* valid pairs to generated HIC file and COOL file when compared
425 the chromatin contact heatmaps or pile-up analysis of E-P/P-P interactions between different methods or
426 samples in this study.

427 The normalization methods used for 3D data can be divided into explicit and implicit approaches
428 according to the principle. Implicit approaches assume that each bin has same sequencing coverage.
429 NicE-C combined NicE-seq and *in situ* Hi-C to efficiently capture chromatin interactions associated
430 with open chromatin regions which was more similar to PLAC-seq (Fang et al. 2016) and HiChIP
431 (Mumbach et al. 2016), which both capture chromatin interactions anchored at genomic regions
432 compared to Hi-C. The matrix-balancing-based normalization methods (ICE, VC, or KR) used for Hi-C
433 data assumed that all genomic regions have equal visibility is invalid for NicE-C and PLAC-seq/HiChIP
434 data as not all the genomic regions are opened or bound by the target proteins.

435 Alternatively, explicit approaches assume that the systematic biases, such as fragment length, GC
436 content and sequence mappability, are known and accounted for in the statistical model. HiCNorm and
437 MAPS are explicit methods used for PLAC-seq and HiChIP data normalization, which generated local
438 genomic features file based on specific restriction endonuclease site and used in data normalization.
439 However, currently, we used Nt.CviPII and DNA Polymerase I for chromatin fragmentation at open
440 chromatin regions in NicE-C, and we found that the chromatin ends generated in NicE-C were not
441 limited to CCD. Due to the NicE-C procedure and the unclear fragmented chromatin ends, the
442 HiCNorm and MAPS were also not suitable for NicE-C data normalization.

443

444 **A/B compartments, TADs and chromatin loops**

445 For comparing the A/B compartments, TADs and chromatin loops in HeLa cells identified by NicE-C
446 and Hi-C, we converted HIC files to HDF5 format as COOL files by cooler (Abdennur and Mirny 2020).
447 Saddle plots of A/B compartments were generated by compute-saddle tool in cooltools
448 (<https://github.com/mirnylab/cooltools>). The upper-left and bottom-right of saddle plot represent the
449 contact frequency between B-B and A-A compartments, the upper-right and bottom-left of saddle plot
450 represent the contact frequency between A and B compartments. Published HeLa TADs and chromatin
451 loops (Rao et al. 2014) were used for pile-up analysis with COOL files generated from NicE-C and Hi-C
452 data. The rescaled pile-up analysis and plot of TADs (1-kb bins) and the pile-up analysis and plot of
453 chromatin loops (1-kb bins) were generated by coolpup.py (Flyamer et al. 2020). High confidence
454 interactions in HeLa NicE-C data were identified using cLoops (Cao et al. 2020) with parameters -eps
455 1000,2000 -minPts 10 -w -j -cut 2000 -s -max_cut -plot.

456

457 **Pile-up analysis of open chromatin interactions**

458 Genome-wide open chromatin interactions between promoter-promoter (P-P), promoter-enhancer (P-E),
459 and enhancer-enhancer (E-E) were assessed by pile-up analysis such as the pile-up analysis of chromatin
460 loops described above. The COOL files of Hi-C, NicE-C, and published Trac-looping (Lai et al. 2018)
461 or OCEAN-C (Li et al. 2018) data were generated by cooler. The cell- and tissue-specific enhancers
462 were identified with published H3K4me3 and H3K27ac ChIP-seq data. The pile-up analysis of P-P, P-E,
463 and E-E interactions were performed with coolpup.py.

464

465 **Chromatin random conversion ratio count**

466 NicE-C, Ocean-C and Trac-looping valid pairs were used for counting chromatin random conversion
467 ratio. The number of hybrid valid pairs with ends from Nuclear DNA (n) and Mitochondrion DNA (m)
468 was denoted by N_{nm} . Total valid pairs number was denoted by N_{total} . We calculated ratio of chromatin
469 random conversion by N_{nm}/N_{total} .

470

471 **TAD boundary analysis and genome-wide distance vs. counts plot**

472 For TAD boundary analysis for HeLa cells, we converted HIC file of Hi-C data to HDF5 format as
473 COOL file by cooler (Abdennur and Mirny 2020). Then, we used the hicFindTADs function in
474 HiCEXplorer (Ramírez et al. 2018) for TAD boundary identification. We only used *cis* chromatin
475 contacts for genome-wide distance vs. counts plot. The COOL files at 1-kb resolution were generated by
476 cooler. Then, the genomic distance vs. chromatin counts plots were plotted by hicPlotDistVsCounts
477 function in HiCEXplorer (Ramírez et al. 2018) with the COOL files.

478

479 **ENCODE and GEO data**

480 ENCODE ChIP-seq and DNase-seq tracks displayed with chromatin contact heatmaps were loaded in
481 Juicebox under the following accession numbers: ENCFF00YCP (IMR-90, CTCF ChIP-seq),
482 ENCFF001LKR (mouse kidney, male, CTCF ChIP-seq), ENCFF000STL (IMR-90, DNase-seq),

483 ENCF247YYB (HeLa S3, DNase-seq), ENCF001PNU (mouse kidney, male, DNase-seq),
484 ENCF000SLH (GM12878, DNase-seq) and ENCF000SEP (CD4⁺ T, human, DNase-seq). Other
485 ChIP-seq, ATAC-seq and RNA-seq tracks displayed with chromatin contact heatmaps were downloaded
486 from the NCBI Gene Expression Omnibus (GEO; <https://www.ncbi.nlm.nih.gov/geo/>) under the
487 following accession numbers: GSM4112813 (HeLa, CTCF ChIP-seq), GSM4112814 (HeLa, CTCF
488 ChIP-seq), GSM2830381 (HeLa, ATAC-seq), GSM2830382 (HeLa, ATAC-seq), GSM5014656
489 (IMR-90, RNA-seq), GSM5014657 (IMR-90, RNA-seq), GSM3965459 (GM12878, RNA-seq),
490 GSM3965460 (GM12878, RNA-seq), GSM2326184 (CD4⁺ T, human, RNA-seq) and GSM2326185
491 (CD4⁺ T, human, RNA-seq).

492

493 **Data access**

494 All raw and processed sequencing data generated in this study have been submitted to the NCBI Gene
495 Expression Omnibus (GEO; <https://www.ncbi.nlm.nih.gov/geo/>) under accession number GSE176066.

496

497 **Competing interest statement**

498 The authors declare that they have no competing interests.

499

500 **Acknowledgments**

501 This work was supported by Research project of Joint Laboratory of University of Science and
502 Technology of China and Anhui mental health center (2019LH03), the Fundamental Research Funds for
503 the Central Universities (WK2070210004) and China Postdoctoral Science Foundation (2021M703091).

504 *Author contributions:* Z.L., R.Z., T.H., and X.S. developed the method. Z.L., R.Z., and T.H.
505 performed experiments. Z.L. and R.Z. analyzed the data. Z.L., R.Z., T.H., Y.Z, and X.S. wrote the
506 manuscript. All authors discussed the results and edited the manuscript.

507

508 **References**

- 509 Abdennur N, Mirny LA. 2020. Cooler: scalable storage for Hi-C data and other genomically labeled
510 arrays. *Bioinformatics* **36**: 311-316.
- 511 Anders S, Pyl PT, Huber W. 2015. HTSeq--a Python framework to work with high-throughput
512 sequencing data. *Bioinformatics* **31**: 166-169.
- 513 Banigan EJ, van den Berg AA, Brandão HB, Marko JF, Mirny LA. 2020. Chromosome organization by
514 one-sided and two-sided loop extrusion. *eLife* **9**: e53558.
- 515 Bonev B, Mendelson Cohen N, Szabo Q, Fritsch L, Papadopoulos GL, Lubling Y, Xu X, Lv X, Hugnot
516 J-P, Tanay A et al. 2017. Multiscale 3D Genome Rewiring during Mouse Neural Development.
517 *Cell* **171**: 557-572.e524.
- 518 Buenrostro JD, Giresi PG, Zaba LC, Chang HY, Greenleaf WJ. 2013. Transposition of native chromatin
519 for fast and sensitive epigenomic profiling of open chromatin, DNA-binding proteins and
520 nucleosome position. *Nature Methods* **10**: 1213-1218.
- 521 Cao Y, Chen Z, Chen X, Ai D, Chen G, McDermott J, Huang Y, Guo X, Han JJ. 2020. Accurate loop
522 calling for 3D genomic data with cLoops. *Bioinformatics* **36**: 666-675.

- 523 Chin HG, Sun Z, Vishnu US, Hao P, Cejas P, Spracklin G, Esteve PO, Xu SY, Long HW, Pradhan S.
524 2020. Universal NicE-seq for high-resolution accessible chromatin profiling for
525 formaldehyde-fixed and FFPE tissues. *Clin Epigenetics* **12**: 143.
- 526 Cho SW, Xu J, Sun R, Mumbach MR, Carter AC, Chen YG, Yost KE, Kim J, He J, Nevins SA et al.
527 2018. Promoter of lncRNA Gene PVT1 Is a Tumor-Suppressor DNA Boundary Element. *Cell*
528 **173**: 1398-1412 e1322.
- 529 Durand NC, Robinson JT, Shamim MS, Machol I, Mesirov JP, Lander ES, Aiden EL. 2016. Juicebox
530 Provides a Visualization System for Hi-C Contact Maps with Unlimited Zoom. *Cell Systems* **3**:
531 99-101.
- 532 Fang R, Yu M, Li G, Chee S, Liu T, Schmitt AD, Ren B. 2016. Mapping of long-range chromatin
533 interactions by proximity ligation-assisted ChIP-seq. *Cell Research* **26**: 1345-1348.
- 534 Flyamer IM, Illingworth RS, Bickmore WA. 2020. Coolpup.py: versatile pile-up analysis of Hi-C data.
535 *Bioinformatics* **36**: 2980-2985.
- 536 Fudenberg G, Imakaev M, Lu C, Goloborodko A, Abdennur N, Mirny Leonid A. 2016. Formation of
537 Chromosomal Domains by Loop Extrusion. *Cell Reports* **15**: 2038-2049.
- 538 Giresi PG, Lieb JD. 2009. Isolation of active regulatory elements from eukaryotic chromatin using
539 FAIRE (Formaldehyde Assisted Isolation of Regulatory Elements). *Methods* **48**: 233-239.
- 540 Hsieh TS, Cattoglio C, Slobodyanyuk E, Hansen AS, Rando OJ, Tjian R, Darzacq X. 2020. Resolving
541 the 3D Landscape of Transcription-Linked Mammalian Chromatin Folding. *Mol Cell* **78**:
542 539-553 e538.
- 543 Hua JT, Ahmed M, Guo H, Zhang Y, Chen S, Soares F, Lu J, Zhou S, Wang M, Li H et al. 2018a. Risk
544 SNP-Mediated Promoter-Enhancer Switching Drives Prostate Cancer through lncRNA PCAT19.
545 *Cell* doi:10.1016/j.cell.2018.06.014.
- 546 Hua JT, Ahmed M, Guo H, Zhang Y, Chen S, Soares F, Lu J, Zhou S, Wang M, Li H et al. 2018b. Risk
547 SNP-Mediated Promoter-Enhancer Switching Drives Prostate Cancer through lncRNA PCAT19.
548 *Cell* **174**: 564-575 e518.
- 549 Isoda T, Moore AJ, He Z, Chandra V, Aida M, Denholtz M, Piet van Hamburg J, Fisch KM, Chang AN,
550 Fahl SP et al. 2017. Non-coding Transcription Instructs Chromatin Folding and
551 Compartmentalization to Dictate Enhancer-Promoter Communication and T Cell Fate. *Cell* **171**:
552 103-119 e118.
- 553 Javierre BM, Burren OS, Wilder SP, Kreuzhuber R, Hill SM, Sewitz S, Cairns J, Wingett SW, Varnai C,
554 Thiecke MJ et al. 2016. Lineage-Specific Genome Architecture Links Enhancers and
555 Non-coding Disease Variants to Target Gene Promoters. *Cell* **167**: 1369-1384 e1319.
- 556 Krietenstein N, Abraham S, Venev SV, Abdennur N, Gibcus J, Hsieh T-HS, Parsi KM, Yang L, Maehr
557 R, Mirny LA et al. 2020. Ultrastructural Details of Mammalian Chromosome Architecture.
558 *Molecular Cell* doi:<https://doi.org/10.1016/j.molcel.2020.03.003>.
- 559 Lai B, Tang Q, Jin W, Hu G, Wangsa D, Cui K, Stanton BZ, Ren G, Ding Y, Zhao M et al. 2018.
560 Trac-looping measures genome structure and chromatin accessibility. *Nat Methods* **15**: 741-747.
- 561 Langmead B, Salzberg SL. 2012. Fast gapped-read alignment with Bowtie 2. *Nat Methods* **9**: 357-359.

- 562 Li D, Hsu S, Purushotham D, Sears RL, Wang T. 2019. WashU Epigenome Browser update 2019.
563 *Nucleic Acids Research* **47**: W158-W165.
- 564 Li T, Jia L, Cao Y, Chen Q, Li C. 2018. OCEAN-C: mapping hubs of open chromatin interactions
565 across the genome reveals gene regulatory networks. *Genome Biol* **19**: 54.
- 566 Lieberman-Aiden E, Van Berkum NL, Williams L, Imakaev M, Ragozy T, Telling A, Amit I, Lajoie
567 BR, Sabo PJ, Dorschner MO. 2009. Comprehensive mapping of long-range interactions reveals
568 folding principles of the human genome. *science* **326**: 289-293.
- 569 Love MI, Huber W, Anders S. 2014. Moderated estimation of fold change and dispersion for RNA-seq
570 data with DESeq2. *Genome Biol* **15**: 550.
- 571 Mifsud B, Tavares-Cadete F, Young AN, Sugar R, Schoenfelder S, Ferreira L, Wingett SW, Andrews S,
572 Grey W, Ewels PA et al. 2015. Mapping long-range promoter contacts in human cells with
573 high-resolution capture Hi-C. *Nature Genetics* **47**: 598-606.
- 574 Mumbach MR, Rubin AJ, Flynn RA, Dai C, Khavari PA, Greenleaf WJ, Chang HY. 2016. HiChIP:
575 efficient and sensitive analysis of protein-directed genome architecture. *Nature Methods* **13**: 919.
- 576 Pertea M, Kim D, Pertea GM, Leek JT, Salzberg SL. 2016. Transcript-level expression analysis of
577 RNA-seq experiments with HISAT, StringTie and Ballgown. *Nature Protocols* **11**: 1650-1667.
- 578 Ponnaluri VKC, Zhang G, Esteve PO, Spracklin G, Sian S, Xu SY, Benoukraf T, Pradhan S. 2017.
579 NicE-seq: high resolution open chromatin profiling. *Genome Biol* **18**: 122.
- 580 Quinlan AR, Hall IM. 2010. BEDTools: a flexible suite of utilities for comparing genomic features.
581 *Bioinformatics* **26**: 841-842.
- 582 Ramírez F, Bhardwaj V, Arrigoni L, Lam KC, Grüning BA, Villaveces J, Habermann B, Akhtar A,
583 Manke T. 2018. High-resolution TADs reveal DNA sequences underlying genome organization
584 in flies. *Nature Communications* **9**: 189.
- 585 Ramírez F, Dündar F, Diehl S, Grüning BA, Manke T. 2014. deepTools: a flexible platform for
586 exploring deep-sequencing data. *Nucleic Acids Res* **42**: W187-191.
- 587 Rao SS, Huntley MH, Durand NC, Stamenova EK, Bochkov ID, Robinson JT, Sanborn AL, Machol I,
588 Omer AD, Lander ES et al. 2014. A 3D map of the human genome at kilobase resolution reveals
589 principles of chromatin looping. *Cell* **159**: 1665-1680.
- 590 Servant N, Varoquaux N, Lajoie BR, Viara E, Chen CJ, Vert JP, Heard E, Dekker J, Barillot E. 2015.
591 HiC-Pro: an optimized and flexible pipeline for Hi-C data processing. *Genome Biol* **16**: 259.
- 592 Song L, Crawford GE. 2010. DNase-seq: a high-resolution technique for mapping active gene regulatory
593 elements across the genome from mammalian cells. *Cold Spring Harbor protocols* **2010**:
594 [pdb.prot5384](http://www.ncbi.nlm.nih.gov/pmc/articles/PMC2931664/).
- 595 Takemon Y, Chick JM, Gerdes Gyuricza I, Skelly DA, Devuyst O, Gygi SP, Churchill GA, Korstanje R.
596 2021. Proteomic and transcriptomic profiling reveal different aspects of aging in the kidney.
597 *eLife* **10**: e62585.
- 598 Weintraub AS, Li CH, Zamudio AV, Sigova AA, Hannett NM, Day DS, Abraham BJ, Cohen MA,
599 Nabet B, Buckley DL et al. 2017. YY1 Is a Structural Regulator of Enhancer-Promoter Loops.
600 *Cell* **171**: 1573-1588 e1528.

601 Yang T, Zhang F, Yardimci GG, Song F, Hardison RC, Noble WS, Yue F, Li Q. 2017. HiCRep:
 602 assessing the reproducibility of Hi-C data using a stratum-adjusted correlation coefficient.
 603 *Genome Res* **27**: 1939-1949.

604 Zhang Y, Liu T, Meyer CA, Eeckhoute J, Johnson DS, Bernstein BE, Nusbaum C, Myers RM, Brown
 605 M, Li W et al. 2008. Model-based analysis of ChIP-Seq (MACS). *Genome Biol* **9**: R137.

606

607 **Figure Legends**

608 **Figure 1. NicE-C discovers open chromatin associated chromatin interactions.** (A) Schematic of the
 609 NicE-C method. (B) A snapshot of chromatin accessibility detected by NicE-C, NicE-seq, and published
 610 ATAC-seq data for HeLa cells. (C) Venn diagram of open chromatin peaks identified by NicE-C,
 611 NicE-seq, and published ATAC-seq data. (D, E) HeLa NicE-C (D) and Hi-C (E) chromatin contact maps
 612 of an example region on Chromosome 1 at 1-kb resolution. Snapshots of 1D chromatin tracks (ChIP-seq
 613 of CTCF, H3K4me3 and H3K27ac, DNase-seq (see Methods for references), open chromatin signal of
 614 NicE-C and NicE-seq) in this region are also shown. Numbers below the interaction maps correspond to
 615 the maximum signal in the matrix. (F) Genome-wide averaged pile-up matrices (plotted at 1-kb
 616 resolution, windows = 200 kb) showing promoter-promoter/promoter-enhancer interactions (P-P/E-P
 617 loops) and stripes detected by NicE-C (HeLa) and Hi-C (HeLa).

618

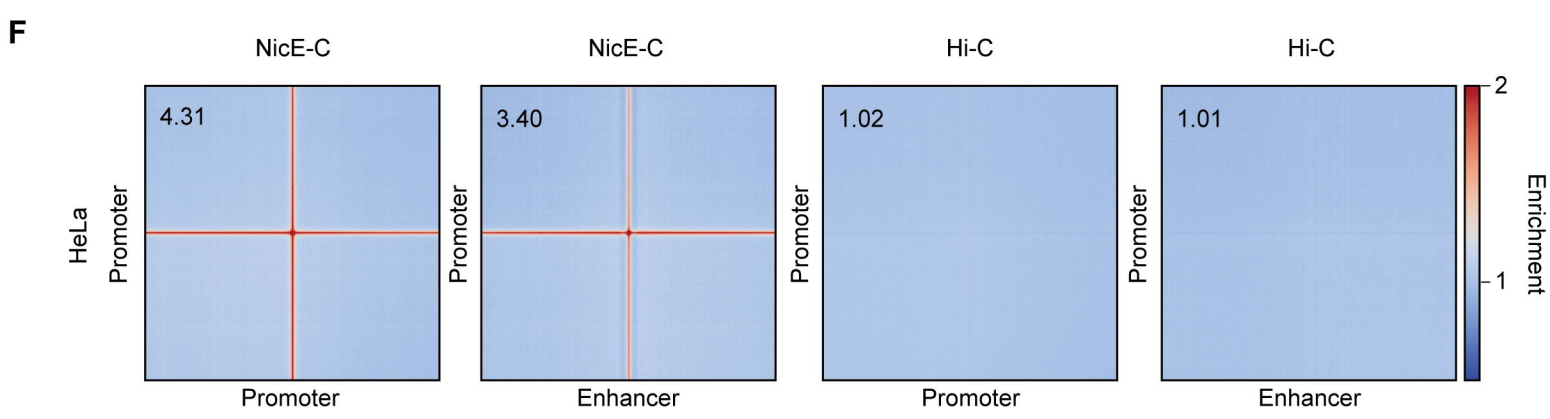
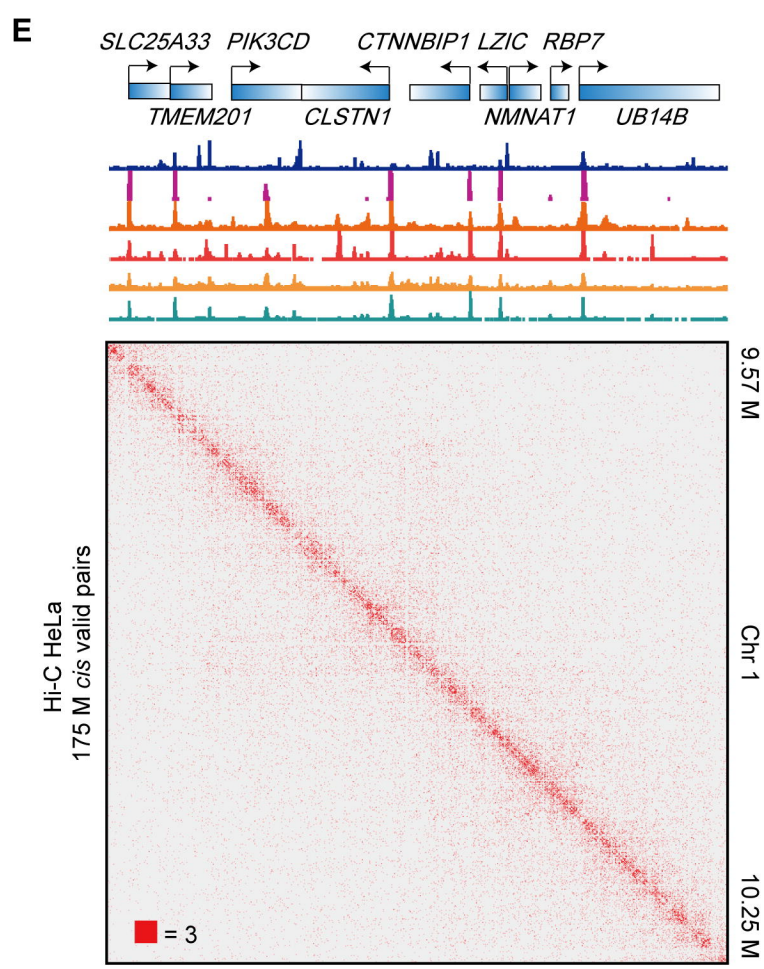
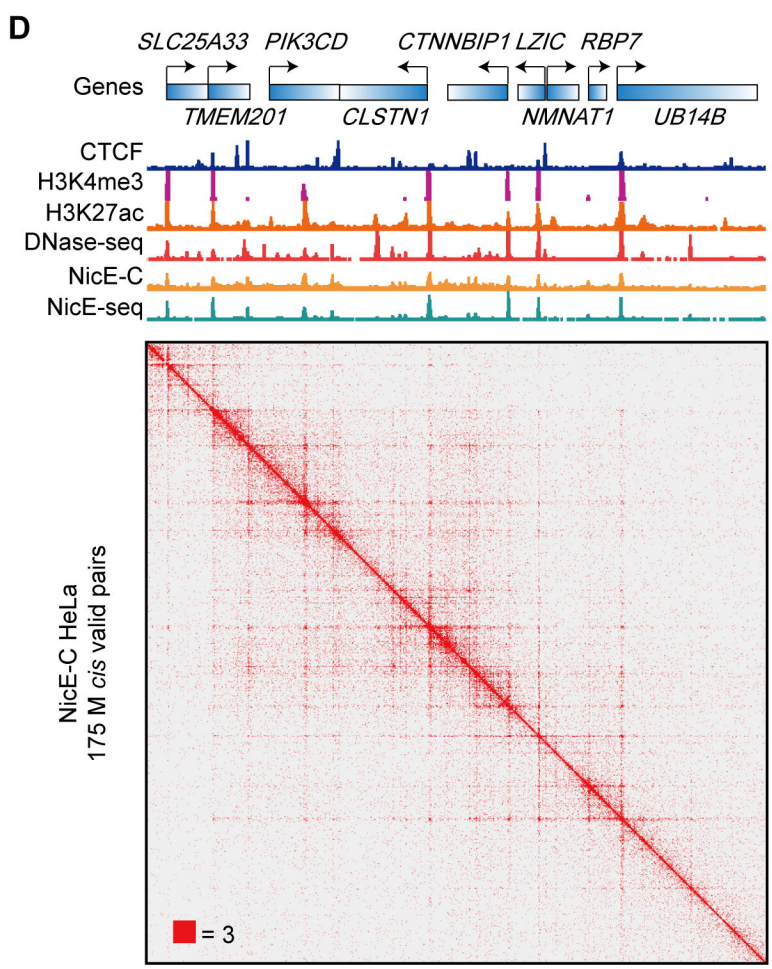
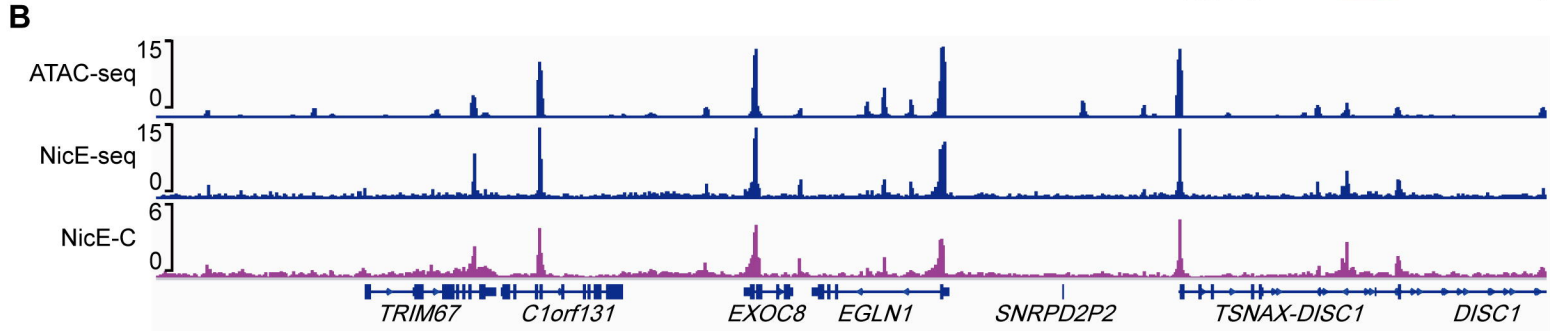
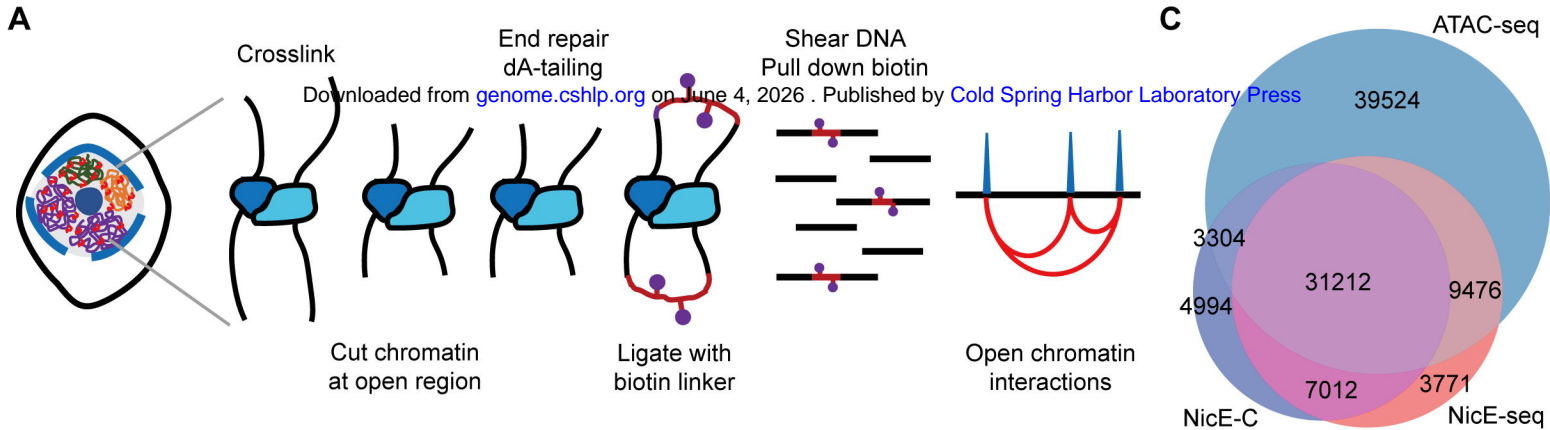
619 **Figure 2. Open chromatin interactions captured by NicE-C, Trac-looping, and OCEAN-C.** (A-D)
 620 HeLa cells NicE-C (A), IMR-90 cells NicE-C (B), CD4⁺ T cells Trac-looping (C), and GM12878 cells
 621 OCEAN-C (D) chromatin contact maps of an example region (TPM value of *JAK* gene for these four
 622 cells are ~120) on Chromosome 1 at 1-kb resolution. Heatmaps were plotted with equal *cis* valid pairs.
 623 The RefSeq genes, RNA-seq and DNase-seq signal of four different cell lines are also shown. (E)
 624 Genome-wide averaged pile-up matrices (plotted at 1-kb resolution, windows = 200 kb) showing P-P
 625 interactions and stripes detected by NicE-C (HeLa cells and IMR-90 cells), Trac-looping (CD4⁺ T cells),
 626 OCEAN-C (GM12878 cells), and Hi-C (HeLa cells).

627

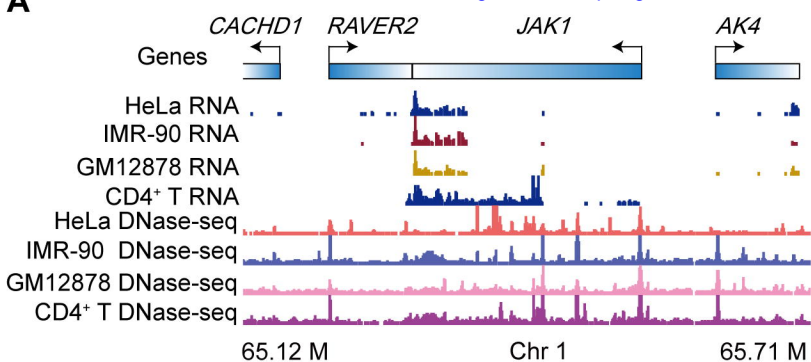
628 **Figure 3. Comparison of NicE-C with 1 M and 0.1 M HeLa S3 cells.** (A) PCR duplication rates of
 629 NicE-C (~ 420 M reads) with 1 M and 0.1 M input cells. (B) Venn diagram of open chromatin peaks
 630 identified by NicE-C with 1 M and 0.1 M input cells. (C) Reproducibility analysis of 1 M cells and 0.1
 631 M cells NicE-C data. Reproducibility scores were calculated by HiC-Rep at different resolutions. (D)
 632 NicE-C chromatin contact maps of an example region on Chromosome 2 at 1-kb resolution, the top right
 633 of the heatmap showed the NicE-C data with 1 M input cells, the bottom left of the heatmap showed the
 634 NicE-C with 0.1 M input cells. Snapshots of 1D chromatin tracks (ChIP-seq of CTCF, H3K4me3 and
 635 H3K27ac, open chromatin signals of NicE-C and DNase-seq) in this region are also shown. Numbers
 636 below the interaction maps correspond to maximum signal in the matrix. (E) Genome-wide averaged
 637 pile-up matrices of P-P, E-E, and E-P loops and stripes were plotted at 1-kb resolution (windows = 200
 638 kb). The top plots showed NicE-C data with 0.1 M input cells while the bottom plots showed NicE-C
 639 data with 1 M input cells.

640

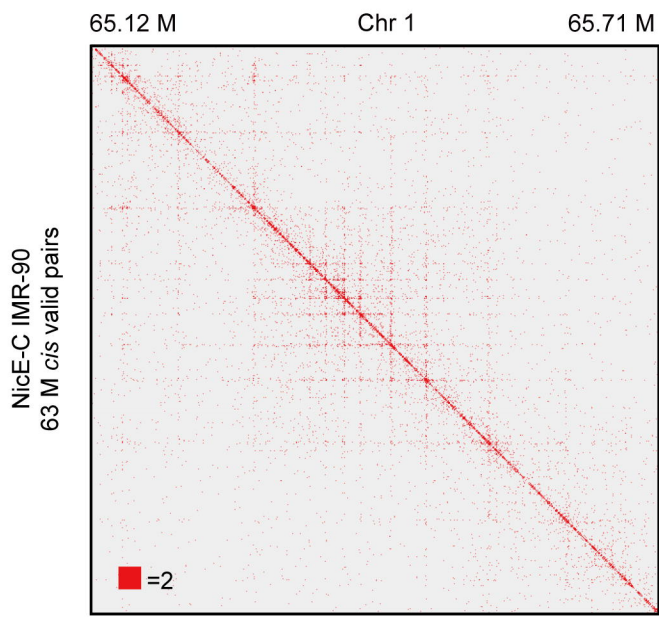
641 **Figure 4. Dynamic enhancer-promoter interactions detected by NicE-C.** (A) An example of
642 TNF-stimulation induced changes in E-P loops around the *TNFAIP3* locus, detected by NicE-C.
643 Snapshots of 1D chromatin tracks (ChIP-seq of H3K4me3 and H3K27ac, and DNase-seq (see Methods
644 for references); open chromatin signals of NicE-C, and RNA-seq) in the example region are also shown.
645 Red arrows pointing to e1 to e6 show the putative enhancers based on ChIP-seq, DNase-seq, and our
646 NicE-C peaks. The region in orange represents the gene promoter. Ovals indicate examples of increased
647 interactions associated with indicated gene promoter in TNF treated cells compared to control cells. (B)
648 An example of E-P loops in old mouse kidney compared to those in young mouse kidney around the
649 *AcsM3* locus (down-regulated gene in old mouse kidney), detected by NicE-C. Snapshots of 1D
650 chromatin tracks (ChIP-seq of H3K4me3 and H3K27ac, DNase-seq, open chromatin signals of NicE-C
651 and RNA-seq) in this region are also shown. Red arrows pointing to e1 to e4 show the putative
652 enhancers based on ChIP-seq, DNase-seq, and our NicE-C peaks. The region in orange represents the
653 gene promoter. Ovals indicate examples of decreased interactions associated with indicated gene
654 promoter in old kidney compared to young kidney.



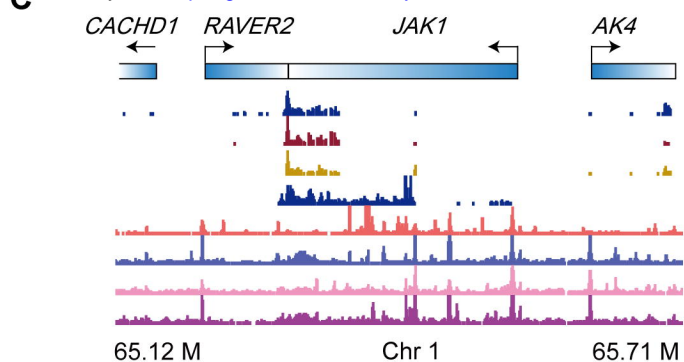
A



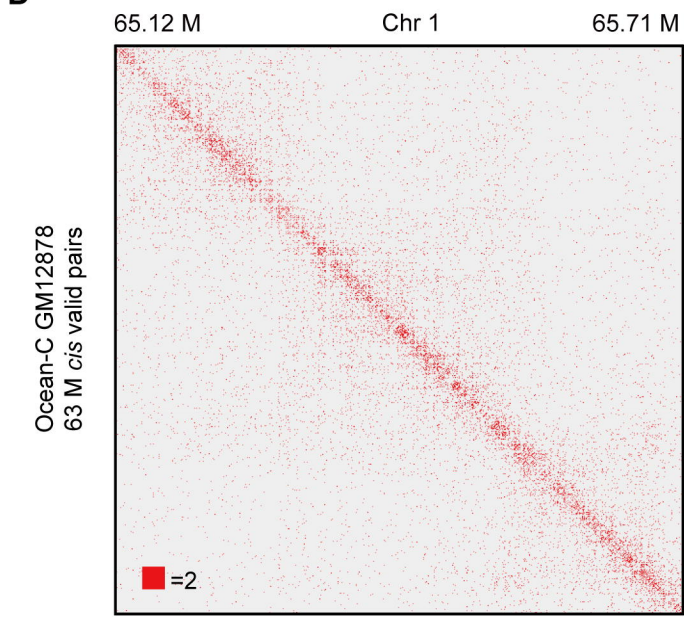
B



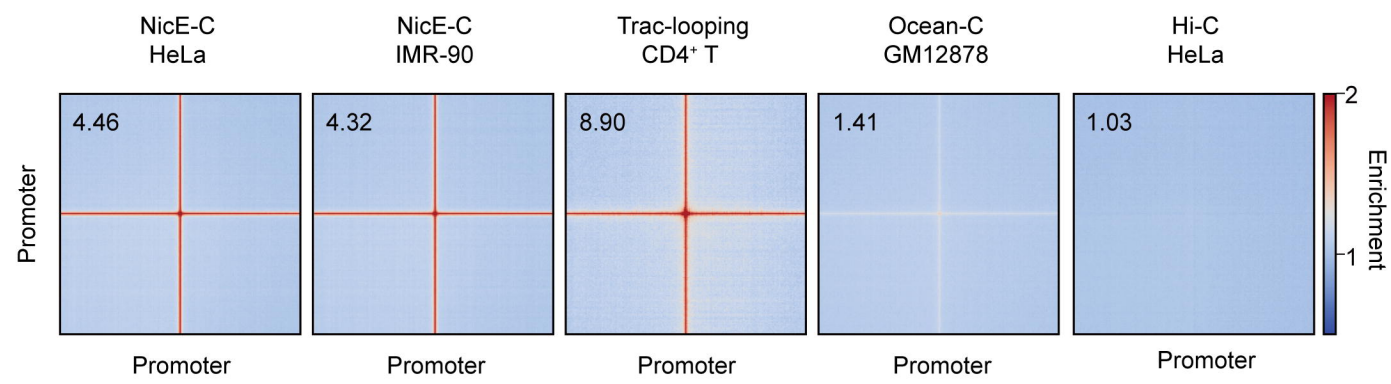
C

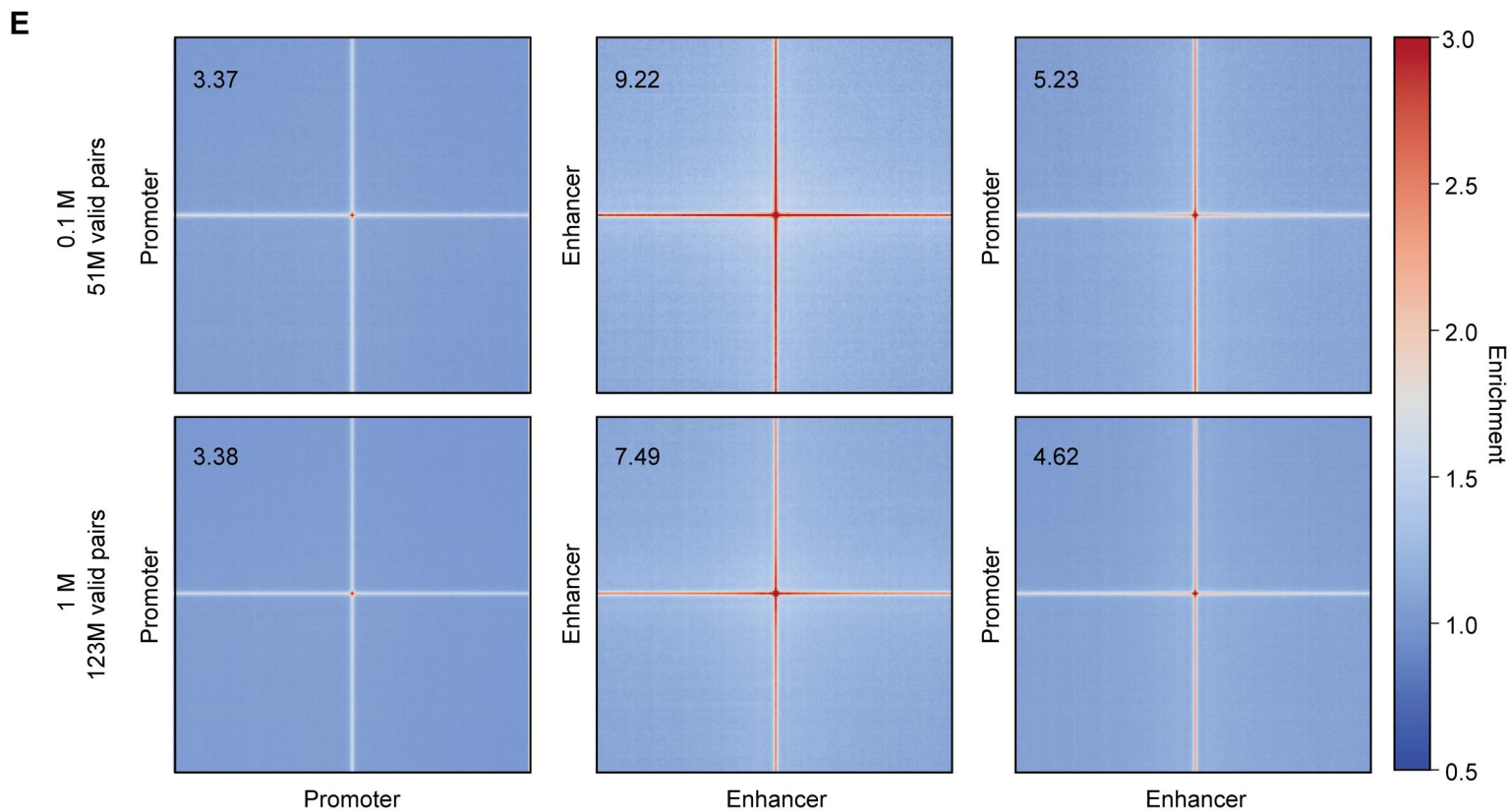
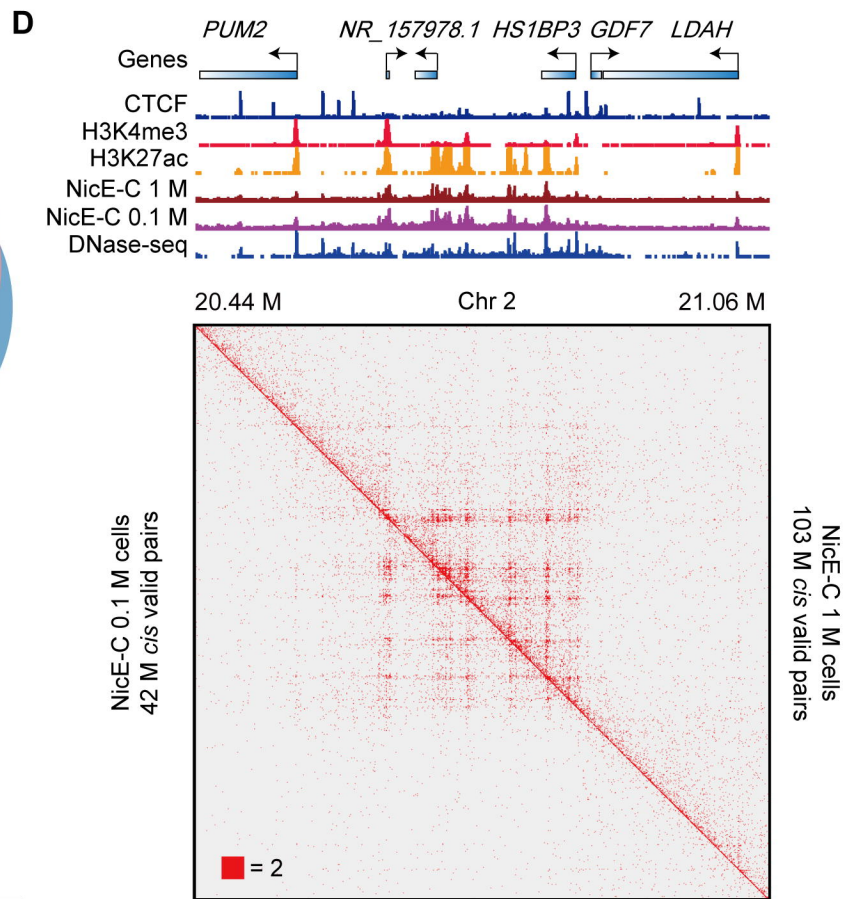
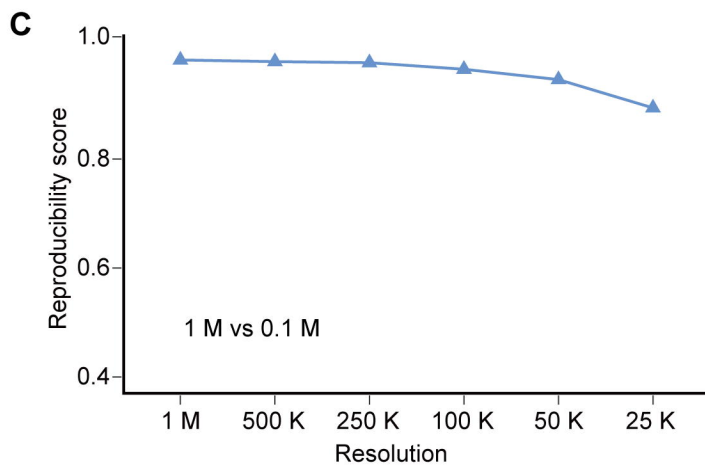
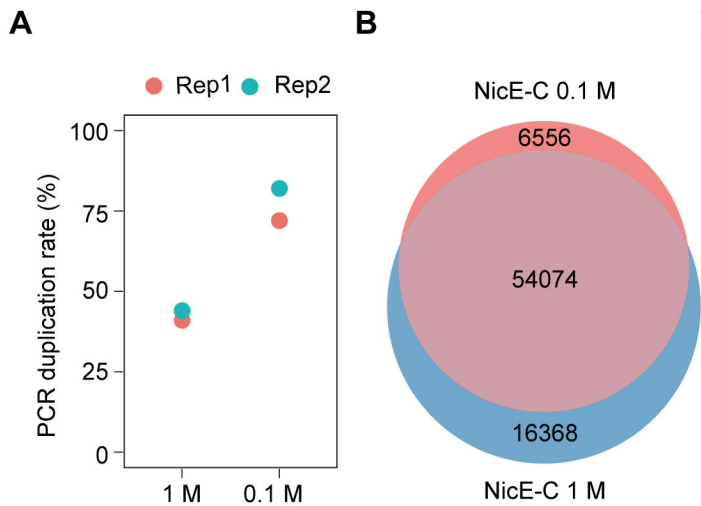


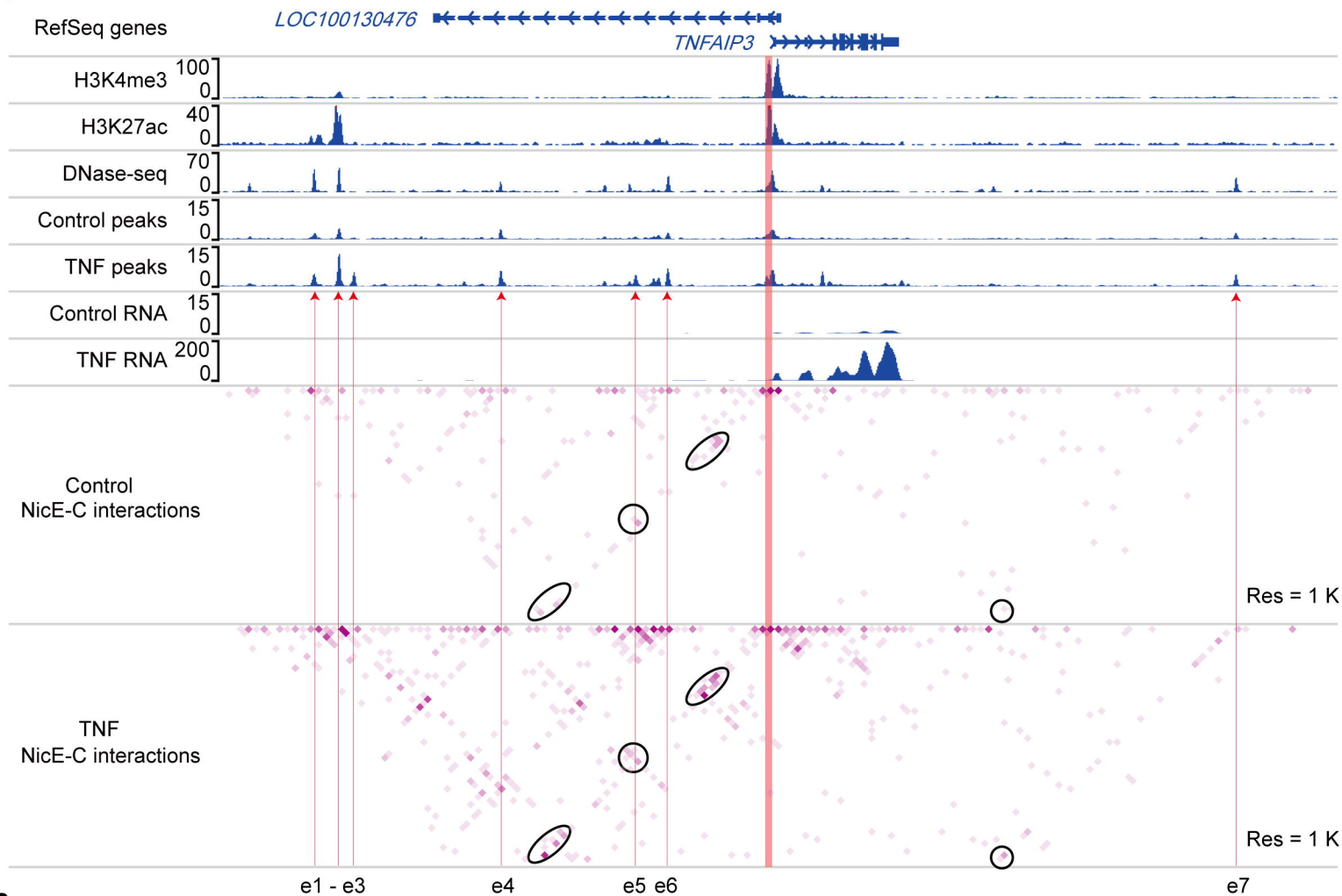
D



E





A**B**